ISSN (Print) 1226-1750
ISSN (Online) 2233-6656
Journal of Magnetics 27(1), 88-95 (2022) https://doi.org/10.4283/JMAG.2022.27.1.088

Influences of Postannealing Treatment Parameters on the Structural and Magnetic Properties of Nickel-Doped Cobalt Ferrite Synthesized by Sol-Gel Route

Sri Budiawanti[1], R. Amalia[2], D. T. Rahardjo[1], Suharno[1], B. Purnama[2]*, and D. Djuhana[3]

[1]Physics Education Department, Faculty of Teacher Training and Education, Universitas Sebelas Maret, Jl. Ir. Sutami 36A Kentingan, Jebres, Surakarta 57126, Indonesia
[2]Physics Department, Faculty of Mathematics and Natural Sciences, Universitas Sebelas Maret, Jl. Ir. Sutami 36A Kentingan, Jebres, Surakarta 57126, Indonesia
[3]Physics Department of Universitas Indonesia, Physics Department, Faculty of Mathematics and Natural Sciences, Universitas Indonesia, Kampus Baru UI Depok, 16424, Indonesia

(Received 30 October 2021, Received in final form 23 March 2022, Accepted 24 March 2022)

We prepared and characterized nickel-substituted cobalt ferrite ($Ni_{0.1}Co_{0.9}Fe_2O_4$) nanoparticles using the sol-gel method. The physical properties of the nanoparticles have been modified by postannealing treatment at atmospheric conditions. X-ray diffraction results confirmed that the nanoparticles possessed a single-phase face-centered cubic crystalline structure. The crystallite sizes increased from 20.85 to 26.06 nm with the increased annealing temperature. Transmission electron microscopy results confirmed the crystal structure of the nickel-substituted cobalt ferrite nanoparticles. Furthermore, Fourier-transform infrared spectroscopy results showed that the typical characteristic absorption of the nanoparticles was obtained at wave numbers $k = 575$ and 374 cm^{-1}. Finally, the saturation magnetization and coercivity of the nanoparticles increased with the annealing temperature, which is attributed to the increase in magnetic anisotropy constant.

Keywords : cobalt ferrite, substituted, nickel, sol-gel, annealing

1. Introduction

Cobalt ferrite ($CoFe_2O_4$) is a magnetic material [1], which has been extensively studied because of its interesting properties, such as medium saturation magnetization (80 emu/g) [2], good mechanical strength and chemical stability, large anisotropy ($\sim \times 10^6$ erg/cm^3), and high coercivity (~5,4 kOe). Cobalt ferrite has been shown to demonstrate superparamagnetic properties [3]. Cobalt ferrite-based materials with superparamagnetic properties have been obtained by modifying the synthesis temperature [4], annealing [5], and metal ion substitution [6]. The modified properties of cobalt ferrite can find biomedical applications [7], particularly in biosensing, cancer treatment, and targeted drug delivery [8]. Additionally, cobalt ferrite-based materials can be applied to magnetorheological ferrofluid systems [9].

Recently, studies have been conducted to deploy cobalt ferrite nanoparticles as carriers for targeted drug delivery [4], which requires a relatively small particle size (< 100 nm) and a coercivity close to 0 (superparamagnetism) [3]. These characteristics can be obtained by nickel substitution [10], synthesis temperature [4], and low-temperature annealing [5]. Ni^{2+} has high permeability, high magnetization intensity, and low coercivity.

Among the physical properties of modified cobalt ferrite-based materials, substitution with nickel is a major concern as it is magnetic. Additionally, nickel-substituted cobalt ferrite has been reported to be sensitive to the synthesis procedure [11, 12]. It is reported that the saturation magnetization and coercivity decreased as the Ni concentration increased by using a sol-gel route [13] as well as the coprecipitation procedure [14]. Here, the decrease in the saturation magnetization and coercivity supported the reduction of magnetic anisotropy [13]. Otherwise, the crystallite size increases as the annealing temperature increases [15]. This trend is also consistent with other ion-doped cobalt ferrite nanoparticles such as strontium and bismuth. Furthermore, the substitution of nickel into cobalt ferrite nanoparticles as a result of

*Corresponding author: Tel: +62-271-669376
Fax: +62-271-663375, e-mail: bpurnama@mipa.uns.ac.id

coprecipitation showed an increase in crystallite size [14], although other papers reported independence to nickel content in cobalt ferrite [16-18]. So that, the changes in the magnetic characteristics described above should be contributed by the redistribution of cations at the octahedral and tetrahedral sites than changes in the microstructure of the nanoparticle sample.

In this study, the synthesis and characterization of nickel-substituted cobalt ferrite nanoparticles were studied using the sol-gel method. Temperature annealing (300 °C, 400 °C, and 500 °C) was conducted to modify the properties of the obtained nanoparticles. The selection of the sol gel procedure followed by a relatively low annealing temperature was intended to modify small nanoparticles for photocatalyst applications [19]. The synthesized nanoparticles were characterized by X-ray diffraction (XRD) to determine their crystal structures, Fourier-transform infrared (FTIR) spectroscopy to determine the oxide bonding groups, and vibrating sample magnetometry (VSM) to determine their magnetic properties.

2. Experimental Procedure

Sample preparation was conducted by the sol-gel method using the following steps: First, (0.001 mol) $Ni(NO_3)_2{\cdot}6H_2O$ (Merck), (0.0099 mol) $Co(NO_3)_2{\cdot}6H_2O$ (Merck), and (0.02 mol) $Fe(NO_3)_2{\cdot}9H_2O$ (Merck) were mixed under magnetic stirring at 300 rpm for 10 min at room temperature. Second, after the homogenous solution was obtained, 0.056 mol $C_6H_8O_7{\cdot}H_2O$ (Merck) was mixed with the previous solution, and the final solution was heated at 80 °C under magnetic stirring at a rotational speed of 300 rpm. The procedure ended upon gel formation. Thereafter, the gel formed was placed in an oven at 150 °C for 1 h to dry completely. After cooling to room temperature, samples were pounded using a mortar for 1 h. Finally, postannealing was performed in atmospheric condition at 300 °C, 400 °C, and 500 °C for 4 h before sample characterization. The obtained samples of $Ni_{0.1}Co_{0.9}Fe_2O_4$ were characterized using XRD, FTIR, and VSM. XRD PAN alytical type X'pert Pro (Cu Kα source with $\lambda = 1.5406$ Å) was used to detect the crystalline structure of the samples. FTIR spectroscopy (Shimadzu IR Prestige 21) was used to determine oxide bond groups in the synthesized samples. VSM (Oxford 1.2) was used to determine the magnetic properties of the samples.

Furthermore, the crystallite size D was calculated using the most intense peak, which belonged to the (311) surface, and the Scherrer equation [20]:

$$D = \frac{k\lambda}{\beta\cos\theta'} \tag{1}$$

where λ is the wavelength of the Cu Kα source, θ is diffraction angle and β refers to the full width at half-maximum of the (311) peak. The lattice parameter (a) was obtained using Equation [17]:

$$a = d_{hkl}\sqrt{h^2 + k^2 + l^2} \tag{2}$$

where a (Å) is the lattice parameter [21]. The crystalline density was calculated by

$$d_x = \frac{8M}{Na^3}, \tag{3}$$

where M is the molecular weight, N is Avogadro's number, a is the lattice parameter, and d_x is the density. The density is inversely proportional to the volume of the crystallite [22].

The lattice strain was calculated using the Williamson-Hall equation [15]:

$$\varepsilon = \frac{\beta_{hkl}}{4\tan\theta}, \tag{4}$$

where ε is the strain and β_{hkl} refers to the full width at half-maximum of the (311) peak.

The force constant was calculated using Equation [3]:

$$k_0 = 10.62 \times M_2/2 \times k_2^2 \times 10^{-7}\ \text{N/m} \tag{5}$$

$$k_t = 7.62 \times M_1 \times k_1^2 \times 10^{-7}\ \text{N/m} \tag{6}$$

where k_t is the tetrahedral force constant, k_o is the octahedral force constant, M_1 and M_2 are the molecular masses of the cations, and k_1 and k_2 are wave numbers. The location of the lattice strain was determined on the basis of changes in k_t and k_o.

3. Results and Discussion

XRD PANalytical type X'pert Pro (Cu Kα source, λ: 1,5406 Å) was used to characterize $Ni_{0.1}Co_{0.9}Fe_2O_4$ samples from 15° to 80° angle. XRD characterization was conducted to determine the crystal structures formed at various annealing temperatures. The lattice parameters, crystal size, density, and crystallite volumes were quantitatively analyzed on the basis of XRD results.

Figure 1(a) shows that the peaks corresponded to ICDD data number 221086, which indicates the formation of the cobalt ferrite phase with Fd3m space group and a face-centered cubic (fcc) crystal structure. Fig. 1(a) shows the most intense peak that corresponded to the (311) surface at $2\theta = 35.57° \pm 0.02°$, which agreed well with ICDD number 221086 ($2\theta = 35.44°$). Fig. 1(b) shows the (311) peak shifts of $Ni_{0.1}Co_{0.9}Fe_2O_4$ samples with variations in annealing temperature. A shift of 0.15, 0.11, and 0.13 for

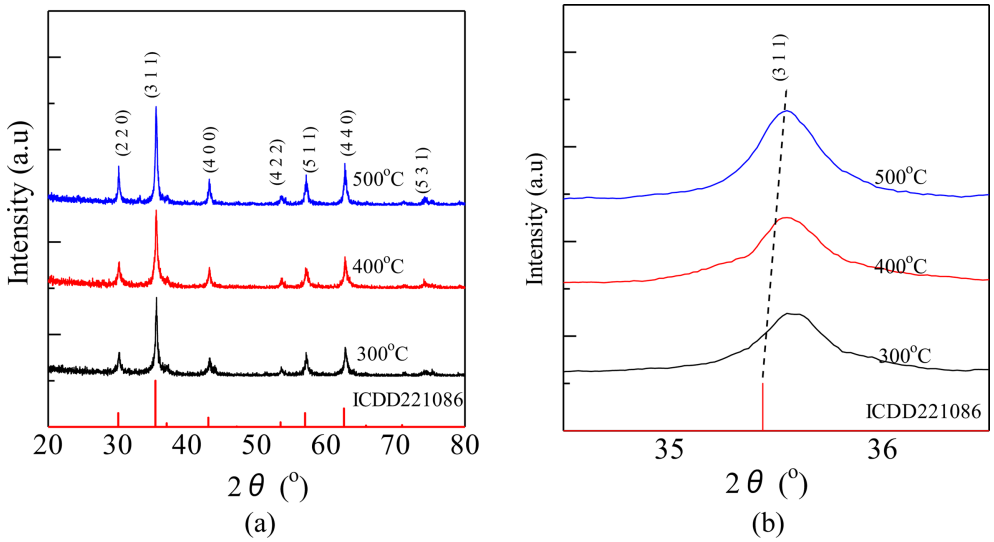

Fig. 1. (Color online) (a) XRD patterns and (b) magnified peaks of the (311) surface of $Ni_{0.1}Co_{0.9}Fe_2O_4$ samples using annealing temperatures of 300 °C, 400 °C, and 500 °C.

annealing temperatures of 300 °C, 400 °C, and 500°C occurred because of the substitution of Co^{2+} ions with Ni^{2+} ions as the Ni^{2+} ion has a smaller radius (0.69 nm) compared with that of the Co^{2+} ion (0.74 nm) [23]. However, in this study, the peak shift was caused by the lattice constant change according to Equations 2.3 and 3.4. The difference in lattice constants is due to changes in annealing temperature. Table 1 shows the shifts in angle orientation due to annealing temperature treatment.

Quantitative analysis to determine the lattice parameters (a), crystal size (D), density (d_x), and volume of the crystallite (V) was conducted on $Ni_{0.1}Co_{0.9}Fe_2O_4$ samples annealed at 300 °C, 400 °C, and 500 °C, as shown in Table 1.

Table 1 shows that the crystallite sizes of $Ni_{0.1}Co_{0.9}Fe_2O_4$ samples increased with the annealing temperature. The crystallite size increased from 20.85 nm at 300 °C to 26.06 nm at 500 °C. The higher annealing temperature causes the atoms to interact and diffuse to form a larger crystalline. Additionally, the increased annealing temperature accelerates the crystallization process so that larger crystallite sizes can be obtained [24]. These results are according to those reported previously [5]. Fig. 2 shows the relationship between the crystallite sizes of $Ni_{0.1}Co_{0.9}Fe_2O_4$ samples and the annealing temperature.

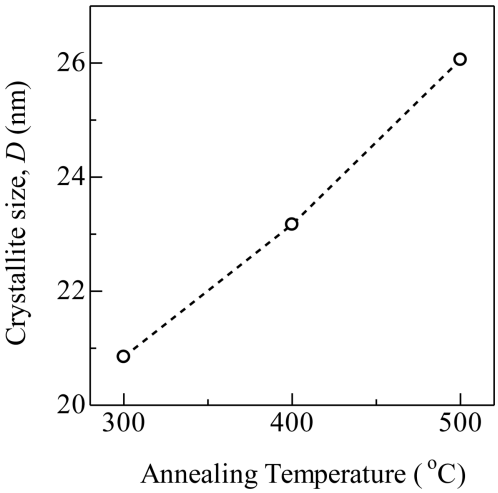

Fig. 2. Annealing temperature-dependent variation in the crystallite size of $Ni_{0.1}Co_{0.9}Fe_2O_4$ nanoparticles.

The lattice parameter of $Ni_{0.1}Co_{0.9}Fe_2O_4$ was found to be higher as the annealing temperature increased and was closer to the value reported in the literature (a = 8.39 Å) [25]. The increase in lattice parameters is due to the transfer of Co^{2+} ions from octahedral sites to tetrahedral

Table 1. Crystallite sizes (D), lattice parameters (d), densities (d_x), lattice strains ε, and volume of crystalline $Ni_{0.1}Co_{0.9}Fe_2O_4$ samples prepared at various annealing temperatures.

T (°C)	D (nm)	a (Å)	dx (g/cm^3)	Lattice strain (ε)	Volume of crystallite (Å^3)
300	20.85 ± 0.17	8.369 ± 0.002	5.315 ± 0.004	0.0054	586.243
400	23.17 ± 0.17	8.375 ± 0.001	5.304 ± 0.001	0.0049	587.436
500	26.06 ± 0.18	8.376 ± 0.001	5.302 ± 0.002	0.0043	587.715

Table 2. Wave numbers and tetrahedral (k_t) and octahedral (k_o) force constants of $Ni_{0.1}Co_{0.9}Fe_2O_4$ samples annealed at various temperatures.

T (°C)	k_1 (cm^{-1})	k_2 (cm^{-1})	k_t (N/m)	k_a (N/m)	F (N/m)
300	581.560	357.810	14.394	7.803	11.098
400	576.740	379.030	14.156	8.756	11.456
500	579.630	337.560	14.298	6.945	10.621

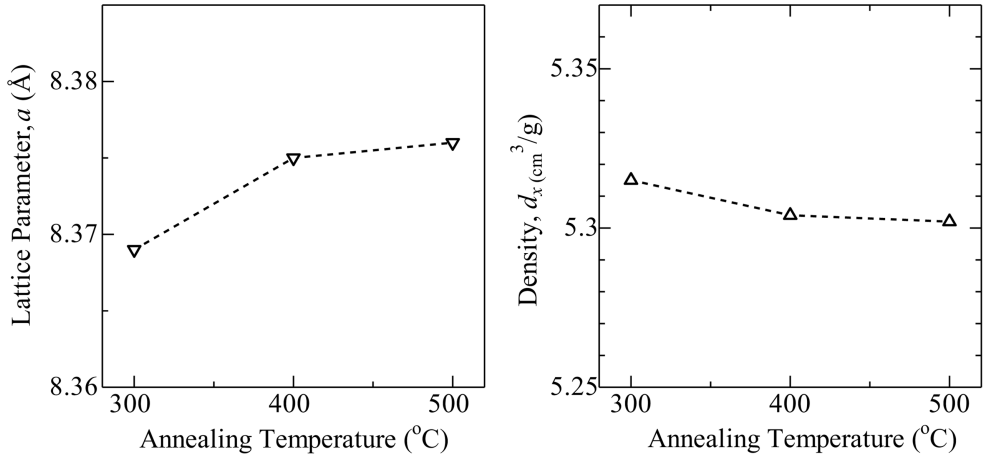

Fig. 3. (a) Relationship between lattice parameters and annealing temperature in $Ni_{0.1}Co_{0.9}Fe_2O_4$ samples. (b) Relationship between density and annealing temperature in $Ni_{0.1}Co_{0.9}Fe_2O_4$ samples.

sites [23]. The decrease in density due to the higher lattice parameters caused by a volume increase [22]. For annealing temperatures of 300 °C, 400 °C, and 500 °C, the samples had density values of 5.315, 5.304, and 5.302 g/cm^3 and lattice parameter values of 8.369, 8.375, and 8.376 Å, respectively. Table 2 shows the calculated data from the lattice parameters, density, and volume of crystallites. Fig. 3 shows the relationship between lattice parameters and density values with the increased annealing temperature of $Ni_{0.1}Co_{0.9}Fe_2O_4$ samples.

The results of the calculation of lattice strain on $Ni_{0.1}Co_{0.9}Fe_2O_4$ samples decreased from 0.0054 to 0.0043 when the annealing temperature increased from 300 °C to 500 °C. The decrease in the value of lattice strain can be associated with an increase in crystallite size. Fig. 4 shows the relationship between the lattice strain and the annealing temperature.

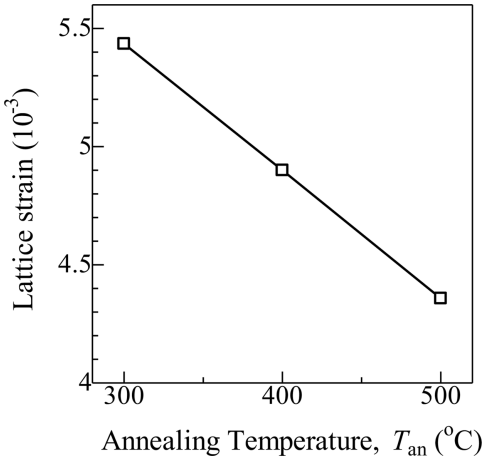

Fig. 4. Lattice strain versus annealing temperature for $Ni_{0.1}Co_{0.9}Fe_2O_4$ samples.

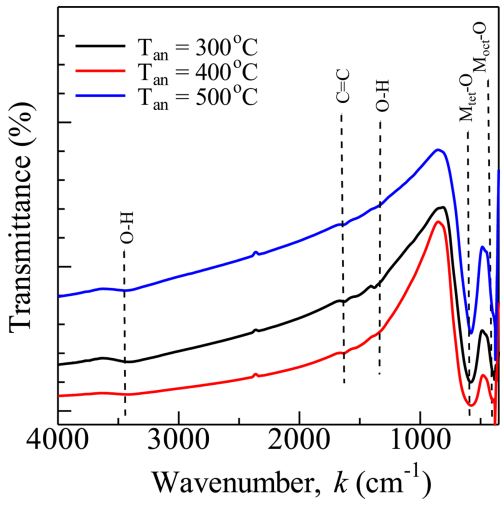

Fig. 5. (Color online) FTIR spectral patterns of $Ni_{0.1}Co_{0.9}Fe_2O_4$ samples annealed at various temperatures.

Figure 5 shows the FTIR spectral patterns of $Ni_{0.1}Co_{0.9}Fe_2O_4$ samples at various annealing temperatures. No particular trend was formed as a result of changes in the transmittance values with the increased annealing temperature. The results of the absorption band obtained in this study are in accordance with the study conducted by Waldron [26]. In the FTIR spectral pattern, the characteristic absorption curve of cobalt ferrite can be seen at wave numbers between 575 and 374 cm^{-1}. The highest transmittance was observed for the sample annealed at 500 °C.

The face centered cubic has four FTIR bands, which represent two basic absorption bands, namely, the low-frequency bands (k_2) and high-frequency bands (k_2) [27]. The absorption band with a high frequency is considered as bending vibration octahedral metal complex comprising bonds between oxygen ions and metal ions at the octahedral site, whereas the absorption band with a low

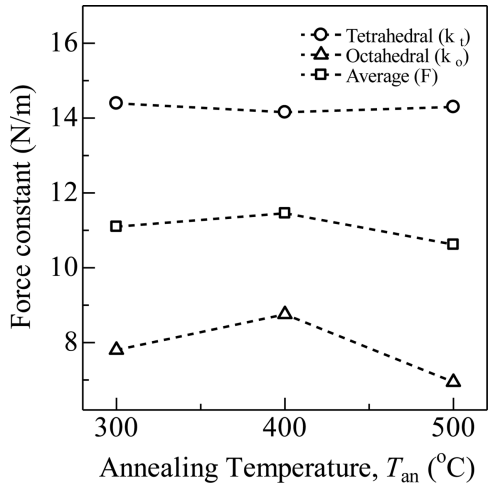

Fig. 6. Force constants at tetrahedral (k_t) and octahedral (k_o) sites of $Ni_{0.1}Co_{0.9}Fe_2O_4$ with variations in annealing temperature.

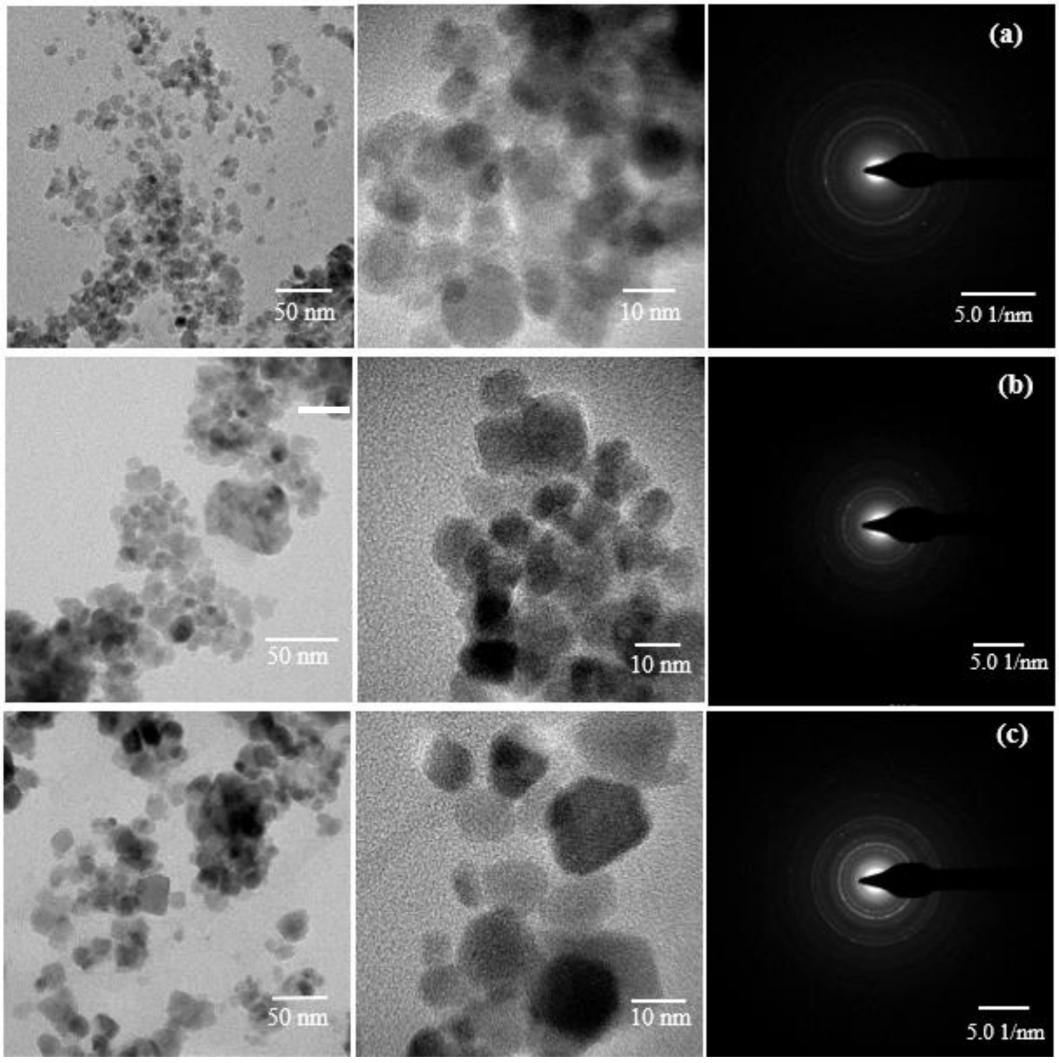

Fig. 7. TEM, HR-TEM, and SAED for nickel-substituted cobalt ferrite with three different annealing temperatures of 300 °C, 400 °C, and 500 °C.

frequency is considered as stretching vibration of a metal-tetrahedral complex. At this frequency, it comprises bonds between oxygen ions and metal ions at tetrahedral sites. From the research, the absorption band with the highest frequency is in the range of 576.74-581.56 cm^{-1}, whereas the absorption band with the lowest frequency is in the range of 337.56-380.03 cm^{-1}.

Table 2 shows the wave numbers and the force constants at the tetrahedral (k_t) and octahedral (k_o) sites of the $Ni_{0.1}Co_{0.9}Fe_2O_4$ samples annealed at various temperatures. Table 4.3 shows that the characterization presents the same trend between k_1 and k_2 with the increased annealing temperature, although they have different frequencies. The difference in frequency between k_1 and k_2 is caused by changes in the bond length of Fe^{3+}-O^{2-} in octahedral and tetrahedral sites.

Besides the frequency band, Table 2 shows the value of the force constant at the octahedral and tetrahedral sites. The force constant depends on the atomic number of the metal, the oxygen ion, and the distance between the metal ion and the oxygen ion [23]. The difference in the force constant with variations in the annealing temperature (300 °C, 400 °C, and 500 °C) is due to the shift in the wave number, which affects the bonding of metal ions and oxygen ions. The decrease in the force constant at the octahedral site is due to the substitution of Ni^{2+} ions causing the relocation of Fe^{3+} ions from the octahedral sites to the tetrahedral sites. This causes the ionic radius of the octahedral site to increase; hence, the bond weakens [28]. Fig. 6 shows the relationship between the force constants at octahedral and tetrahedral sites with variations in the annealing temperature of $Ni_{0.1}Co_{0.9}Fe_2O_4$.

Figure 7 shows the results of TEM, HR-TEM, and selected area electron diffraction (SAED) pattern results of nickel-substituted cobalt ferrite nanoparticles annealed at 300 °C, 400 °C, and 500 °C for 4 h under atmospheric conditions. The SAED results further confirm that a fine crystalline structure of the nano powder nickel cobalt ferrite is obtained in the experiment. Other, the TEM results showed that the nanoscale order in magnetic nanoparticles (smaller than 30 nm) has been realized as a result of our sol-gel procedure. At a lower annealing temperature (300 °C), the fine grain size was obtained; then, the grain size gradually increased with the increase in the annealing temperature. Furthermore, the HR-TEM results showed that when the annealing temperature was relatively low, single spherical grains dominated, and when the annealing temperature increased, the morphology slightly became rectangular. These results are consistent with previously reported studies. Furthermore, the results of the EDX evaluation confirmed that the composition of the samples obtained was compatible with the stoichiometric calculations of $Co_{0.9}Ni_{0.1}Fe_2O_4$, i.e., $Co_{0.9}Ni_{0.1}Fe_{2.2}O_{2.7}$; $Co_{0.9}Ni_{0.1}Fe_{2.6}O_{3.3}$, and $Co_{0.9}Ni_{0.9}Fe_{2.1}O_{3.1}$, respectively, for annealing temperatures of 300 °C, 400 °C, and 500 °C, respectively.

Figure 8(a) shows the M–H curve of the nickel-substituted cobalt ferrite nanoparticles annealed at 300 °C, 400 °C, and 500 °C. Fig. 8(b) shows the enlargement of the hysteresis curve in the vertical direction. Table 2 summarizes the calculation of the magnetic parameters. It is clearly observed that the saturation magnetization M_S was 36.50 and 36.65 emu/g for annealing temperatures of 300 °C and 400 °C and then increased to 44.35 emu/g for the annealing temperature of 500 °C. These results are correlated with the calculated magnetic moments of the magnetic nanoparticle samples, which were 1.53, 1.54, and 1.87 for annealing temperatures of 300 °C, 400 °C,

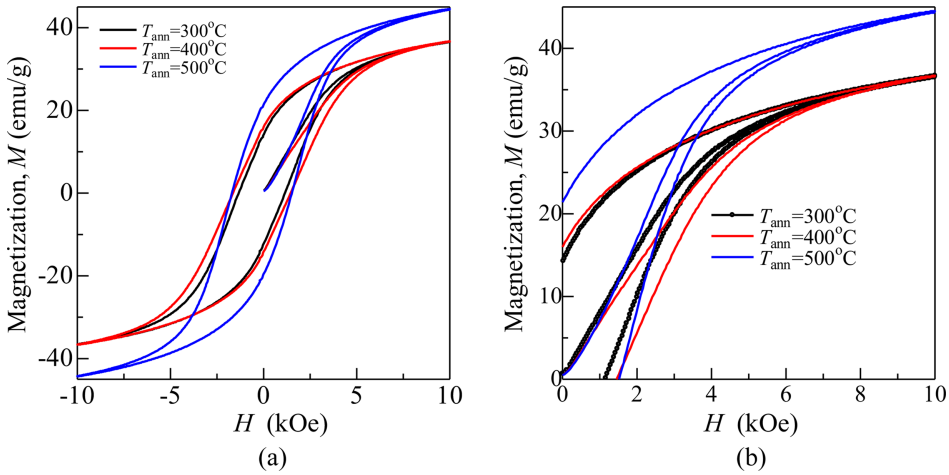

Fig. 8. (Color online) (a) M-H hysteresis loop and (b) magnification of M-H hysteresis loop of $Ni_{0.1}Co_{0.9}Fe_2O_4$ annealed at various annealing temperatures.

Table 3. Remanent magnetization, saturation magnetization, sample coercivity, magnetic moment, and magnetocrystalline anisotropy of $Ni_{0.1}Co_{0.9}Fe_2O_4$ at various annealing temperatures.

T (°C)	M_S (emu/g)	Mr (emu/g)	Hc (Oe)	μ (μ_B)	K_1 ($\times 10^5$ erg/cm^3)
300	36.50	13.10	1235	1.53	2.49
400	36.65	15.00	1550	1.54	3.13
500	44.35	20.40	1600	1.87	3.92

and 500 °C, respectively.

The increase in *Ms* is associated with cation redistribution between the tetrahedral and octahedral sites because of the increase in the annealing temperature. In this case, Fe^{3+} ions migrate to the octahedral site, whereas Co^{2+} occupies the tetrahedral site. Because the magnetic moment of Fe^{3+} ions was greater than that of Co^{2+} ions, the redistribution of Fe^{3+} ions in octahedral sites increases the total magnetic moment, which appears as an increase in *Ms* [15]. This is also supported by the FTIR analysis data, which indicated a redistribution of cations along with the increase in annealing temperature characterized by a shift in the absorption peak of metal oxide bonds at octahedral and tetrahedral sites [20]. The total magnetic moment magnitude of nickel-substituted cobalt ferrite can be expressed as $m_{Tot} = m_{Octa} - m_{Tet}$ [10].

From Table 4, it was known that the annealing temperature influenced the coercivity value (*Hc*). The results showed that *Hc* increased from 1235 Oe at 300 °C to 1550 Oe at 400 °C, reaching its highest value at 500 °C (1600 Oe). This increase in coercivity is due to the crystallite size of the sample and the increase in domain wall pinning caused by structural defects. The presence of Ni^{2+} ion substitution in cobalt ferrite was also found to influence the coercivity magnitude, which could be explained by the domain structure, strain, and magnetic anisotropy constant, $K = (H_C \cdot M_S)/0.98$ [29]. Finally, the increase in the magnetic anisotropy constant (i.e., 2.49×10^5 erg/cm^3, 3.13×10^5 erg/cm^3, and 3.92×10^5 erg/cm^3) contributed to the increase in *Hc*.

4. Conclusion

$Ni_{0.1}Co_{0.9}Fe_2O_4$ nanoparticles were synthesized using the sol-gel auto combustion method. XRD results showed that $Ni_{0.1}Co_{0.9}Fe_2O_4$ had an fcc crystal structure with space group Fd3m. The increase in the annealing temperature resulted in a shift in the (311) peak, an increase in crystallite size and lattice parameters, and a decrease in density and lattice strain. TEM results confirmed the nanocrystalline structure of nickel-substituted cobalt ferrite. The typical characteristic absorption peaks of nickel-substituted cobalt ferrite were obtained at wave numbers k = 575 and 374 cm^{-1} using FTIR spectroscopy. Finally, VSM results indicated that *Ms* and *Hc* increased with the annealing temperature, which is attributed to the increase in the magnetic anisotropy constant.

Acknowledgments

This study was financially supported by Hibah Pasca Doktor Universitas Indonesia contract number NKB-230/UN2.RST/HKP.05.00/2021.

References

[1] H.-J. Jeon, S.-C. Yi, and S.-G. Oh, Biomaterials **24**, 4921 (2003).
[2] Y. Köseoğlu, M. I. O. Oleiwi, R. Yilgin, and A. N. Kocbay, Ceram. Int. **38**, 6671 (2012).
[3] S. Amiri and H. Shokrollahi, J. Magn. Magn. Mater. **345**, 18 (2013).
[4] E. Hutamaningtyas, Utari, Suharyana, B. Purnama, and A. T. Wijayanta, Journal of the Korean Physical Society **69**, 584 (2016).
[5] R. Arilasita, Utari and B. Purnama, J. Kor. Phy. Soc. **74**, 498 (2019).
[6] K. Maaz, A. Mumtaz, S. K. Hasanain, and A. Ceylan, J. Magn. Magn. Mater. **308**, 289 (2007).
[7] X. H. Li, C. L. Xu, X. H. Han, L. Qiao, T. Wang, and F. S. Li, Nanoscale Research Letters **5**, 1039 (2010).
[8] Mahesh Kumar, P Appa Rao, M. C. Varma, G. S. V. R. K. Choudary, and K. H. Rao, Journal of Modern Physics (2011).
[9] K. C. Nugroho, U. Ubaidillah, R. Arilasita, M. Margono, B. H. Priyambodo, B. Purnama, S. A. Mazlan, and S.-B. Choi, Materials **14**, 3684 (2021).
[10] N. B. Velhal, N. D. Patil, A. R. Shelke, N. G. Deshpande, and V. R. Puri, AIP Adv. **5**, 097166 (2015).
[11] P. A. Vinosha, A. Manikandan, R. Ragu, A. Dinesh, K. Thanrasu, Y. Slimani, and B. Xavier, J. Alloys. Compounds **857**, 157517 (2021).
[12] M. M. Naik, H. S. B. Naik, N. Kottam, M. Vinuth, G. Nagaraju, and M. C. Prabhakara, Journal of Sol-Gel Science and Technology **91**, 578 (2019).
[13] M. Mozaffari, J. Amighian, and E Darsheshdar, J. Magn. Mag. Mater. **350**, 19 (2014).
[14] Kumar, N. Yadav, D. S. Rana, P. Kumar, M. Arora, and

R. P. Pant, J. Magn. Magn. Mater. **394**, 379 (2015).
[15] Purnama, A. T. Wijayanta, Journal of King Saud University-Science **31**, 956 (2019).
[16] K. M. Srinivasamurthy, J. Angadi V, S. P. Kubrin, S. Matteppanavar, D. A. Sarychev, P. M. Kumar, H. W. Azale, and B. Rudraswamy, Ceram. Int. **44**, 9194 (2018).
[17] A. B. Nawale, N. S. Kanhe, S. A. Raut, S. V. Bhoraskar, A. K. Das, and V. L. Mathe, Ceram. Int. **43**, 6637 (2017).
[18] A. Mesbahinia, M. Almasi-Kashi, A. Ghasemi, and A. Ramezani, J. Magn. Magn. Mater. **473**, 161 (2019).
[19] J. Revathi, M. J. Abel, V. Archana, T. Sumithra, R. Thiruneelakandan, and J. Joseph Prince, Physica B: Condensed Matter **587**, 412136 (2020).
[20] R. M. Mohamed, M. M. Rashad, F. A. Haraz, and W. Sigmund, J. Magn. Mag. Mater. **322**, 2058 (2010).
[21] W. D. Callister and D. G. Rethwisch, Materials Science and Engineering: an Introduction, John Wiley & Sons. Inc, New York (2007) pp. 665-715.
[22] S. Nasrin, F. U. Z. Chodhury, and S. M. Hoque, J. Magn. Mag. Mater. **479**, 126 (2019).
[23] E. A. Setiadi, S. Simbolon, M. Yunus, C. Kurniawan, A. P. Tetuko, S. Zelviani, and P. Sebayang, J. Physics **9791**, 012064 (2018).
[24] C. S. Kumar and F. Mohammad, Advanced Drug Delivery Reviews **63**, 789 (2011).
[25] M. Houshiar, F. Zebhi, Z. J. Razi, A. Alidoust, and Z. Askari, J. Magn. Magn. Mater. **371**, 43 (2014).
[26] R. D. Waldron, Physical Review. **99**, 1727 (1955).
[27] B. G. Toksha, S. E. Shirsath, S. M. Patange, and K. M. Jadhav, Solid State Communications **147**, 479 (2013).
[28] P. P. Hankare, K. R. Sanadi, K. M. Garadkar, D. R. Patil, and I. S. Mulla, J. Alloys. Comp. **553**, 383 (2013).
[29] G. S. Kumar, T. Raguram, and K. S. Rajni, Journal of Superconductivity and Novel Magnetism **32**, 1715 (2019).